GRANT NUMBER DAMD17-98-1-8302

TITLE: Compact Gamma Camera System for Breast Cancer Imaging

PRINCIPAL INVESTIGATOR: Stephen E. Derenzo, Ph.D.

CONTRACTING ORGANIZATION: University of California at Berkeley
                          Berkeley, California 94720

REPORT DATE: July 1999

TYPE OF REPORT: Annual

PREPARED FOR: Commanding General
                U.S. Army Medical Research and Materiel Command
                Fort Detrick, Maryland 21702-5012

DISTRIBUTION STATEMENT: Approved for Public Release;
                          Distribution Unlimited

The views, opinions and/or findings contained in this report are those of the author(s) and should not be construed as an official Department of the Army position, policy or decision unless so designated by other documentation.

REPORT DOCUMENTATION PAGE

Form Approved
OMB No. 0704-0188

Public reporting burden for this collection of information is estimated to average 1 hour per response, including the time for reviewing instructions, searching existing data sources, gathering and maintaining the data needed, and completing and reviewing the collection of information. Send comments regarding this burden estimate or any other aspect of this collection of information, including suggestions for reducing this burden, to Washington Headquarters Services, Directorate for Information Operations and Reports, 1215 Jefferson Davis Highway, Suite 1204, Arlington, VA 22202-4302, and to the Office of Management and Budget, Paperwork Reduction Project (0704-0188), Washington, DC 20503.

1. AGENCY USE ONLY *(Leave blank)*	2. REPORT DATE July 1999	3. REPORT TYPE AND DATES COVERED Annual (1 Jul 98 - 30 Jun 99)

4. TITLE AND SUBTITLE
Compact Gamma Camera System for Breast Cancer Imaging

5. FUNDING NUMBERS
DAMD17-98-1-8302

6. AUTHOR(S)
Stephen E. Derenzo, Ph.D.

7. PERFORMING ORGANIZATION NAME(S) AND ADDRESS(ES)
University of California at Berkeley
Berkeley, California 94720

8. PERFORMING ORGANIZATION REPORT NUMBER

9. SPONSORING / MONITORING AGENCY NAME(S) AND ADDRESS(ES)
U.S. Army Medical Research and Materiel Command
Fort Detrick, Maryland 21702-5012

10. SPONSORING / MONITORING AGENCY REPORT NUMBER

11. SUPPLEMENTARY NOTES

12a. DISTRIBUTION / AVAILABILITY STATEMENT
Approved for Public Release; Distribution Unlimited

12b. DISTRIBUTION CODE

13. ABSTRACT *(Maximum 200 words)*

The goal of this project is the development of a compact solid-state gamma camera specifically designed to image metabolically active tumors in the breast and axillary nodes with the highest possible detection efficiency and spatial resolution.

We have developed or purchased preliminary versions of all major components of the proposed compact solid-state gamma camera: collimators, CsI(Tl) scintillator arrays, special low-noise silicon photodiode arrays, and custom integrated circuit readout chips. Small prototype detector modules were successfully assembled using these components and interfacing them with a computer.

Based on results to date, it appears that our compact camera design will yield very similar performance to traditional SPECT cameras. However, for the application of breast and axillary node imaging, our compact design will have the advantages of: (1) more potential imaging angles, (2) shorter imaging distances and hence higher image quality, and (3) lower cost, making the camera more readily available. Once completed, the new camera may help make scintimammography widely available as a valuable complement to traditional breast cancer screening and diagnostic techniques.

14. SUBJECT TERMS
Breast Cancer

15. NUMBER OF PAGES
17

16. PRICE CODE

17. SECURITY CLASSIFICATION OF REPORT	18. SECURITY CLASSIFICATION OF THIS PAGE	19. SECURITY CLASSIFICATION OF ABSTRACT	20. LIMITATION OF ABSTRACT
Unclassified	Unclassified	Unclassified	Unlimited

FOREWORD

Opinions, interpretations, conclusions and recommendations are those of the author and are not necessarily endorsed by the U.S. Army.

_S.E.D._ Where copyrighted material is quoted, permission has been obtained to use such material.

_S.E.D._ Where material from documents designated for limited distribution is quoted, permission has been obtained to use the material.

_S.E.D._ Citations of commercial organizations and trade names in this report do not constitute an official Department of Army endorsement or approval of the products or services of these organizations.

_____ In conducting research using animals, the investigator(s) adhered to the "Guide for the Care and Use of Laboratory Animals," prepared by the Committee on Care and use of Laboratory Animals of the Institute of Laboratory Resources, national Research Council (NIH Publication No. 86-23, Revised 1985).

_____ For the protection of human subjects, the investigator(s) adhered to policies of applicable Federal Law 45 CFR 46.

_____ In conducting research utilizing recombinant DNA technology, the investigator(s) adhered to current guidelines promulgated by the National Institutes of Health.

_____ In the conduct of research utilizing recombinant DNA, the investigator(s) adhered to the NIH Guidelines for Research Involving Recombinant DNA Molecules.

_____ In the conduct of research involving hazardous organisms, the investigator(s) adhered to the CDC-NIH Guide for Biosafety in Microbiological and Biomedical Laboratories.

Stephen Derenzo   July 29, 1999
PI - Signature   Date

3

4. TABLE OF CONTENTS

5. INTRODUCTION

The goal of this project is the development of a compact solid-state gamma camera specifically designed to image metabolically active tumors in the breast and axillary nodes with the highest possible detection efficiency and spatial resolution. The compact design also allows for a larger number of oblique views and reduces cost, which will make the instrument more widely available to the medical community.

6. BODY OF THE PROGRESS REPORT

Tasks proposed for months 1-12:
- Purchase CsI(Tl) arrays and collimators (months 1-6)
- Fabricate silicon photodiode arrays (months 1-18)
- Fabricate custom integrated circuits containing charge amplifiers and WTA circuits (months 1-18)
- Assemble camera (collimator, crystal arrays, diode arrays, integrated circuit readout, flex strip output connections (months 9-24)

CsI(Tl) Crystal Array

Two CsI(Tl) crystal arrays were acquired, both with an overall size of 12 x 20 cm^2 and with a crystal depth of 5 mm. In the first array the crystal faces are 2.45 x 2.45 mm^2 in size, while in the second they are 3.0 x 3.0 mm^2 (Figure 1). The CsI(Tl) arrays we have acquired can easily be cut into several 8 x 8 element pieces for use in prototype 64-pixel detector modules.

Silicon Photodiode Arrays

Small photodiode arrays, consisting of 12 pixels 3 x 3 mm^2 in size in a 3 x 4 arrangement have been fabricated and tested. During this process the yield per photodiode has been improved from 75% to 99%. The quantum efficiency is greater than 70% at the 540 nm emission wavelength of CsI(Tl), the capacitance is 1.8 pF per element, and the dark current is 20-50 pA per element (this dark current is an order of magnitude better than the best commercially available). At room temperature and a peaking time of 4 μs, the measured noise is as low as 140 e$^-$ rms.

Larger photodiode arrays are now being fabricated and tested as well. The original design called for 256-pixel (16 x 16 element) arrays, but 64 pixels (8 x 8 element) prove a wiser choice. With fewer pixels the yield for entire arrays is greater, and 64-pixel arrays match 1-to-1 to the custom integrated circuit readout chips we are developing. Yield per photodiode for the 64-pixel arrays is 99% with an average dark current in good elements of only 22 pA. The arrays are currently in the process of being diced from their silicon wafers and will then undergo further testing.

Printed Circuit Boards

We have designed and ordered 24 x 24 mm^2 ceramic circuit boards that will be used to mount both the silicon photodiode arrays and our custom integrated circuit readout chips (Figure 2). The circuit boards have 64 contact points that will be connected to the 64 photodiode elements with conductive epoxy. Each of these 64 lines is routed to an area on the other side of the board where they can be wirebonded to the readout chip. A ceramic substrate makes the design and fabrication of this board slightly more challenging, but was chosen nonetheless because it will help minimize the electronic noise in the readout chips.

Custom Integrated Circuit Readout Chip

We have developed a custom integrated circuit chip containing 64 low-noise charge amplifiers and pulse shapers, a 64-channel winner-take-all crystal identifier circuit, address electronics, and computer control of the shaping time and gain of the 64 individual amplifiers (Figure 3). This design was based on two previously developed custom chips, one with 16 charge amplifiers [1], and the other with a 16-input winner-take-all circuit [2]. The 64 input chip is functional, and a second fabrication cycle is being used to produce the final set of readout chips.

The second cycle is well underway, as we have fabricated and vigorously tested two improved versions of the 16-channel chips (one with 16 charge amplifiers and the other with a 16-input winner-take-all circuit). Both have been debugged and been shown to meet the required performance criteria. These two circuits are being combined to produce the final 64-input readout chip.

Collimators

Two lead collimators were acquired (Figure 4). They have hexagonal channels with opening sizes of 1.5 mm and 2.0 mm. They are both 63 x 63 mm^2 in area, and their thickness (which corresponds to the channel length) is 32 mm. These will be suitable for testing completed 24 x 24 mm^2 detector modules.

Integrated Circuit Interconnections

We have designed a multi-layer flex strip that interconnects an 8 x 8 element silicon photodiode array to a 64-channel readout chip and connects the readout chip to a computer interface board.

Detector System Tests

We assembled the following test set-up: (1) one of the collimators describe above, (2) a small CsI(Tl) scintillator array, (3) the 3 x 4 element silicon photodiode array described above, and (4) the 16-element readout chips described above. Data were collected by interfacing with a computer. With this test system, we recorded a pulse height resolution of 10.7% (averaged over all 12 elements in the test set-up) for 140 keV gamma rays from a Tc-99m source (Figure 5). The spatial resolution (including contributions from collimator and detector size) was 5.9 mm fwhm at an imaging distance of 5 cm (Figure 6). When compared to a conventional gamma camera, the energy resolution is only slightly worse and the spatial resolution is approximately two times better. Testing of these small prototype modules is described in greater detail in the attached paper, "A Discrete Scintillation Camera Module Using Silicon Photodiode Readout of CsI(Tl) Crystals for Breast Cancer Imaging" published in *IEEE Trans. Nucl. Sci.*

Simulation and Design Refinement

Monte Carlo simulations were designed and executed to optimize the final camera design. The program includes a phantom patient with different tracer uptake levels in the heart, torso, breast, and tumor (Figure 7). It implements scatter in the patient, collimator geometry, pixel geometry, and detector energy resolution. The simulation results suggest that making pixels smaller than 3.0 x 3.0 mm^2 provides little benefit, that high sensitivity hexagonal hole collimators are a wise choice for this application, and that cooling the electronics below room temperature to lower electronic noise and improve energy resolution is not necessary.

The following tasks were proposed after month 12 and will be described in future progress reports:
- Interface camera to computer (months 18-24)
- Test system using calibration pulses and small ^{57}Co sources (months 20-24)
- Measure intrinsic spatial resolution with and without scatter (months 24-30)
- Measure pulse height resolution with and without scatter (months 24-30)
- Measure planar sensitivity and count rate performance (months 28-36)
- Acquire images of isotope distributions using standard plastic phantoms (months 28-36)

7. KEY RESEARCH ACCOMPLISHMENTS

- Arrays of 64 low-noise silicon photodiodes were fabricated with a yield per photodiode of 99% and an average leakage current in good elements of only 22 pA. Dicing and mounting of the arrays is underway.

- We have developed a functional 64-input custom integrated readout circuit and begun a second fabrication cycle to produce the final set of corrected and improved readout chips. Two distinct 16-input chips form the basic building blocks for the 64-input version, and the final versions of both of those chips have been fabricated and successfully tested.

- Monte Carlo simulation software was developed and used to optimize the final camera design. High sensitivity hexagonal hole collimators and 3.0 x 3.0 mm^2 silicon photodiode/CsI(Tl) scintillator pixels were shown to be wise design choices, while cooling of the electronics in order to lower noise proves unnecessary.

- We have assembled small prototype detector modules comprised of a collimator, a small CsI(Tl) scintillator array, a 12-element low-noise silicon photodiode array, and our two 16-input custom integrated circuit readout chips. These modules demonstrate a pulse height resolution of 10.7% for 140 keV gamma rays from a Tc-99m source and a system spatial resolution of 5.9 fwhm at an imaging distance of 5 cm.

8. REPORTABLE OUTCOMES

G. J. Gruber, W. W. Moses and S. E. Derenzo, "Monte Carlo simulation of breast tumor imaging properties with compact, discrete gamma cameras," presented at the 1998 IEEE Medical Imaging Conference and submitted to *IEEE Trans. Nucl. Sci.*

G. J. Gruber, W. W. Moses, S. E. Derenzo, et al., "A discrete scintillation camera using silicon photodiode readout of CsI(Tl) crystals," *IEEE Trans. Nucl Sci.,* vol. NS-45, pp. 1063–1068, 1998.

N.W, Wang, G. Conti, S.E. Holland, N.P. Palaio, G.J. Gruber, and W.W. Moses, "Improved photosensitive contact for back-illuminated silicon photodiode arrays," presented at the 1998 IEEE Nuclear Science Symposiun and submitted to *IEEE Trans. Nucl. Sci.*

S. E. Holland, N. W. Wang, and W. W. Moses, "Development of low noise, back-side illuminated silicon photodiode arrays," *IEEE Trans. Nucl. Sci.*, vol. NS-44, pp. 443–447, 1997.

9. CONCLUSIONS

We have developed or purchased preliminary versions of all major components of the proposed compact solid-state gamma camera: collimators, CsI(Tl) scintillator arrays, special low-noise silicon photodiode arrays, and custom integrated circuit readout chips. Small prototype detector modules were successfully assembled using these components and interfacing them with a computer. Testing demonstrated both good energy resolution (10.7% for 140 keV) and good spatial resolution (5.9 mm fwhm at 5 cm imaging distance). Final versions of the photodiode arrays and readout chips are currently being developed, with preliminary results for both looking very positive (photodiode yield is 99%, component pieces of the final readout chip work as intended). Monte Carlo simulations have helped optimize the final camera design, supporting the use of high-sensitivity hexagonal hole collimators and 3.0×3.0 mm^2 pixels while demonstrating that cooling the electronics is not necessary.

Based on results to date, it appears that our compact camera design will yield very similar performance to traditional SPECT cameras. However, for the application of breast and axillary node imaging, our compact design will have the advantages of: (1) more potential imaging angles, (2) shorter imaging distances and hence higher image quality, and (3) lower cost, making the camera more readily available. Once completed, the new camera may help make scintimammography a valuable complement to traditional breast cancer screening and diagnostic techniques.

10. REFERENCES

[1] W.W. Moses, I. Kipnis, and M.H. Ho, "A 16-channel charge sensitive amplifier IC for a PIN photodiode array based PET detector module," *IEEE Trans. Nucl. Sci.*, NS-41, pp. 1469–1472, 1994.
[2] W.W. Moses, I. Kipnis, and M.H. Ho, "A 'winner-take-all' IC for determining the crystal of interaction in PET detectors," *IEEE Trans. Nucl. Sci.*, NS-43, pp. 1615–1618, 1996.

11. APPENDICES

**Figures Referenced in Section 6, Body of the Progress Report**

Figure 1. Overhead view of CsI(Tl) scintillator array for use in the compact gamma camera. Individual crystals are $3.0 \times 3.0 \times 5.0$ mm^3 in size and are optically isolated from each other by reflective material (the white grid). Overall array dimensions are 12×20 cm^2, though the array can easily be cut to yield smaller pieces if desired.

(a)   (b)
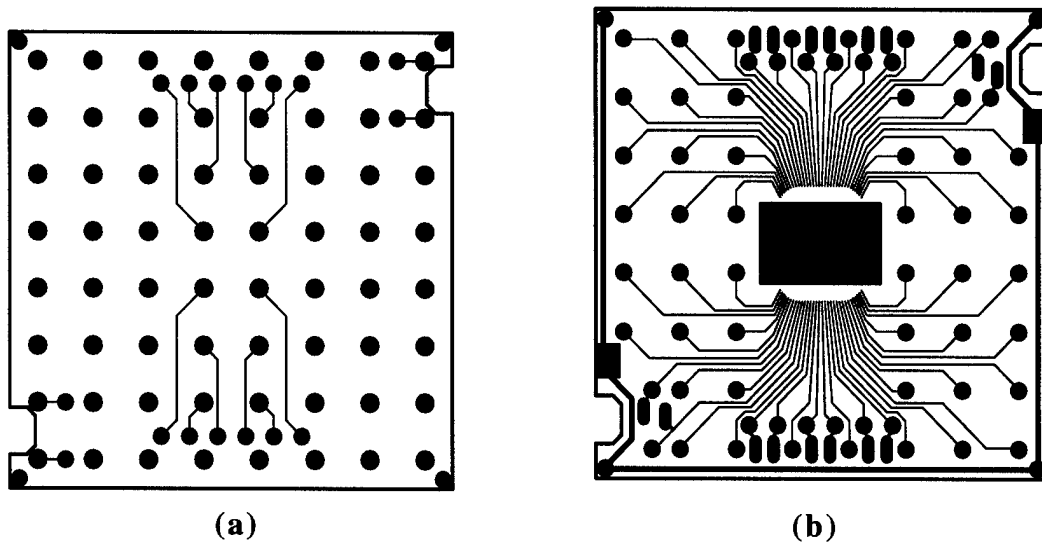
Figure 2. Layout of ceramic printed circuit board used to mount (a) a 64-element photodiode array and (b) a 64-input custom integrated circuit readout chip. Traces route all photodiode signals to allow wirebonding to the readout chip.
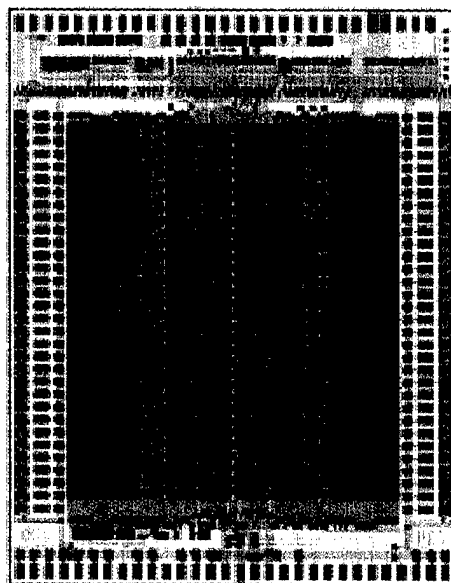

Figure 3. Custom integrated circuit for reading out 64 silicon photodiodes and identifying the largest signal. Chip size is less than 3 x 3 mm^2.
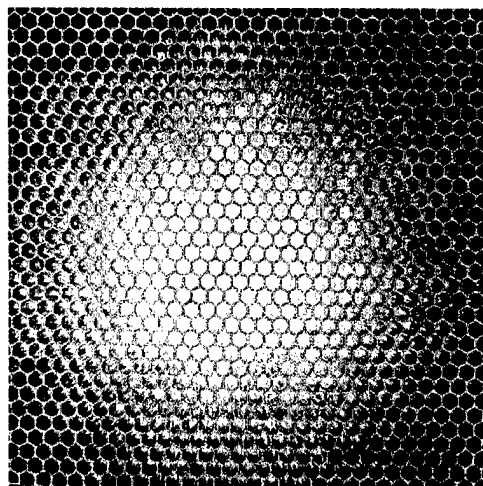
Figure 4. Overhead view of a high-resolution hexagonal hole lead collimator with back-illumination. Individual channels in the collimator are 1.5 mm in diameter and 32 mm in depth, while the septal thickness is 0.2 mm. The complete collimator is 63 x 63 mm^2, suitable for testing prototype detector modules.
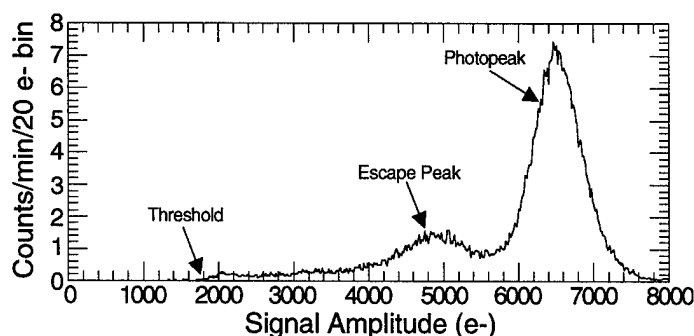

Figure 5. Room temperature Tc-99m photopeak for a typical pixel in a 12-pixel prototype module. Amplifier shaping times were 8 μs rise and 24 μs fall. The signal amplitude is 6530 e- and the photopeak width is 680 e- fwhm, yielding an energy resolution of 10.4% fwhm. The average energy resolution for all twelve array pixels is 10.7±0.6% fwhm.
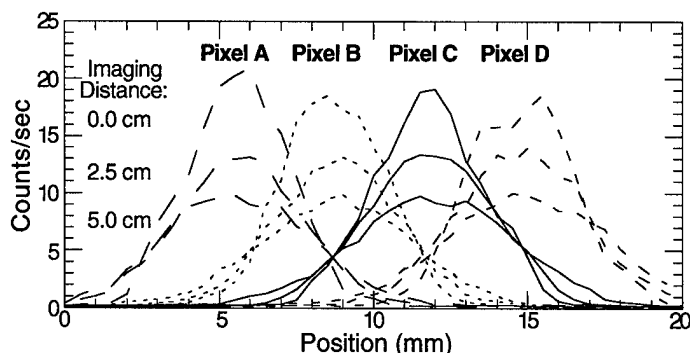
Figure 6. Spatial resolution of a 12-pixel prototype module using a high-resolution hexagonal hole collimator. Shown is the response of the central row of four pixels to a 2.0 mm diameter uncollimated Tc-99m source scanned across at imaging distances of 0.0, 2.5, and 5.0 cm. The average spatial resolution at these distances is 4.1 mm fwhm, 4.8 mm fwhm, and 5.9 mm fwhm, respectively. Measurements were performed in air. The collimator has a sensitivity of 4300 events/mCi/sec.

10
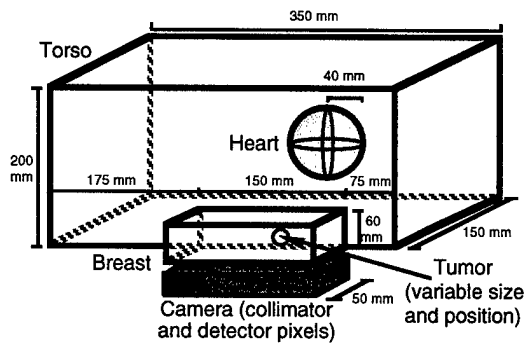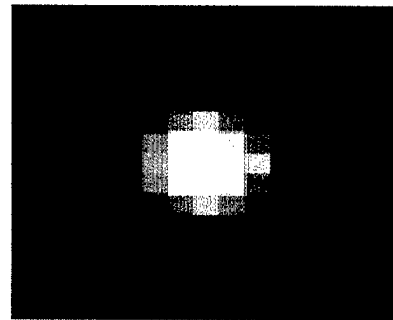
Figure 7. (a) Simulation phantom—including torso, heart, breast, and tumor—used to optimize camera design. The program was used to study the effects of tracer uptake ratios, imaging distance, collimator geometry, detector pixel size, and detector energy resolution. (b) Example image of a simulated tumor generated by the Monte Carlo program. The size and intensity (signal-to-noise) of observed tumors were calculated and compared.

Papers Referenced in Section 6, Body of the Progress Report

G. J. Gruber, W. W. Moses, S. E. Derenzo, et al., "A discrete scintillation camera using silicon photodiode readout of CsI(Tl) crystals," *IEEE Trans. Nucl Sci.,* vol. NS-45, pp. 1063–1068, 1998.

A Discrete Scintillation Camera Module Using Silicon Photodiode Readout of CsI(Tl) Crystals for Breast Cancer Imaging[1]

G.J. Gruber, W.W. Moses, *Senior Member, IEEE,* S.E. Derenzo, *Senior Member, IEEE,* N.W. Wang,
E. Beuville, and M.H. Ho

Lawrence Berkeley National Laboratory, University of California, Berkeley, CA 94720

Abstract

We characterize a 3x4 element imaging array consisting of $3 \times 3 \times 5$ mm^3 CsI(Tl) scintillator crystals individually read out by 3×3 mm^2 PIN silicon photodiodes. The array is a prototype for larger modules (16x16 element) for use in single photon breast cancer imaging. The photodiode output signals are amplified with a 16 channel custom IC (<3 mm on a side), after which a "Winner Take All" (WTA) custom IC (<3 mm on a side) identifies the crystal of interaction based on relative signal amplitudes. The compact nature of these readout electronics will simplify the construction of larger imaging arrays. The photodiodes were developed for low leakage current (~50 pA) and yield a total electronic noise of 390 e- full width at half maximum (fwhm) at a shaping time of 8 μs, with signal levels of 6600 e- for the 140 keV emissions of ^{99m}Tc. Array pixels demonstrate an average room temperature energy resolution of 10.7±0.6% fwhm for these 140 keV gamma rays. We observe an intrinsic spatial resolution of 3.3 mm fwhm for a 2.5 mm diameter ^{57}Co beam on the face of the crystal array, and a system resolution of 5.9 mm fwhm for a 2 mm diameter uncollimated ^{99m}Tc source viewed through a high resolution hexagonal hole collimator (1.5 mm hole diameter, 32 mm length, 4300 events/mCi/sec) at an imaging distance of 5 cm.

I. INTRODUCTION

Recent research has demonstrated that scintimammography imaging with tumor-avid tracers (most commonly ^{99m}Tc-Sestamibi) and standard scintillation cameras can accurately diagnose primary breast cancer, demonstrating sensitivities of 80–94% and specificities of 73–93% [1–4]. Evidence further suggests that this modality performs equally well when imaging radiographically dense breasts [5] and that it shows promise in evaluating the axillary lymph nodes [1, 6–8]. With further development scintimammography could prove a valuable complement to traditional screening techniques.

For this application, compact scintillator/photodiode cameras offer several advantages over conventional scintillation cameras: (1) arrays of small photodiodes provide improved intrinsic spatial resolution; (2) the small camera size allows shorter imaging distances, thus improving collimator resolution; (3) the compact design permits a greater variety of viewing angles and allows multiple cameras to take different views simultaneously; and (4) the multiple scintillator-

photodiode channels yield a higher overall maximum event rate. In this work we characterize a prototype module for a compact camera using optically isolated CsI(Tl) crystals coupled to PIN silicon photodiode arrays. Efforts to develop similar camera technologies are described in references [9–11].

II. DESIGN OVERVIEW

A. Discrete Scintillation Camera Module

The single photon imaging array described in this paper is a prototype for larger modules from which a variety of camera geometries can be realized. A hexagonal hole lead collimator provides directional information, discrete CsI(Tl) crystals convert incident gamma rays to scintillation light, and a photodiode array with custom IC readout detects these scintillation photons. This design is summarized in Figure 1.

The photodiode arrays were designed for low dark current [12], which is critical to minimizing electronic noise at the long shaping times (~8 μs) that are desirable when using CsI(Tl) crystals. At a bias of 50 V, the 3×3 mm^2 photodiodes have typical room temperature characteristics of 50 pA dark current, 4 pF capacitance, and 90% quantum efficiency for the 540 nm emissions of CsI(Tl).

A prototype pixel size of 3×3 mm^2 was chosen as a compromise between several factors. A smaller pixel size both provides slightly better spatial resolution (though this benefit is limited by the fact that the collimator, not pixel size, tends to be the limiting component) and yields lower dark current and capacitance per pixel, which lowers electronic noise. However, using smaller pixels also increases the pixel density and hence the density of electronics required to read out the entire array, which becomes very significant in larger arrays of useful imaging size. Studies on the optimal pixel size for future modules are beyond the scope of this paper.
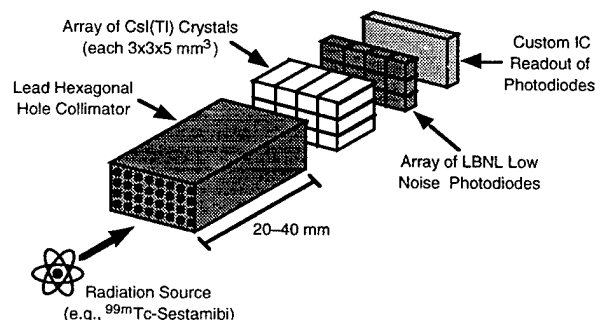
Figure 1: Module of a discrete scintillation camera. The prototype has a 3x4 array of pixels, each composed of a $3 \times 3 \times 5$ mm^3 CsI(Tl) crystal coupled to a 3×3 mm^2 PIN photodiode. The readout circuitry consists of two 3×3 mm^2 ICs. A camera of useful imaging size can be constructed from an array of individual modules.

B. Custom IC Readout of Photodiodes

The photodiode signals are amplified and shaped by a 16 channel charge sensitive integrated circuit (IC) [13], then processed by a 16 channel "Winner Take All" (WTA) IC [14]. The WTA circuit selects the signal with the largest amplitude, thereby determining both the crystal of interaction (pixel address) and the incident photon energy (signal amplitude). The analog "winner" signal selected by the WTA is sent to a threshold discriminator, and the pulse height is read out with a peak detecting CAMAC ADC. At the same time, the six bit digital address computed by the WTA to identify the "winner" channel is read out with a CAMAC I/O board, and both the digitized signal amplitude and the corresponding address are collected by an acquisition computer. This scheme is shown in Figure 2. A 64 channel IC combining both the charge amplifiers and the WTA circuit has been developed and is currently being tested.

The custom ICs used to read out the photodiode signals are less than 3 mm on a side and can be mounted to the back of the photodiode array, allowing for compact design and facilitating the scaling up from a single module to a full camera composed of an array of such modules. Even a small 5x5 cm^2 imaging array would have about 300 channels, making discrete electronics prohibitively bulky.

C. Collimator Selection

Since the collimator is the limiting factor for both spatial resolution and sensitivity in single photon imaging devices, careful collimator design is crucial. Traditional scintillation cameras use hexagonal hole collimators, but in a discrete scintillator camera it is also possible to use square holes matched 1-to-1 (or 4-to-1, etc.) to the square detector pixels. Previous simulations suggest that for square pixel detector arrays, matched square holes provide a superior spatial resolution/sensitivity tradeoff compared to hexagonal holes [15]. Additionally, matching square collimator holes to the detector pixels provides a point spread function with minimal dependence on source position by eliminating the aliasing due to geometric mismatch between hexagonal collimator holes and square detector pixels. Hexagonal hole collimators,
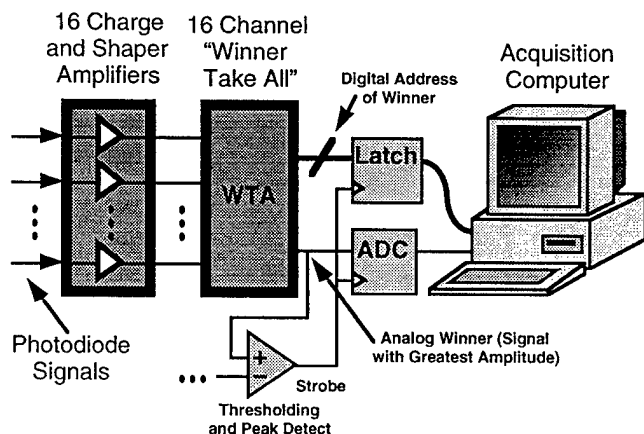

Figure 2. Custom IC readout of photodiode array. The first IC amplifies and shapes the photodiode signals, and the WTA IC selects the signal with the greatest amplitude and passes it plus a six bit digital address denoting the "winner" channel on to an acquisition computer. Both ICs are 3x3 mm in size.

however, have a more symmetric septal penetration pattern and generally result in shorter collimators for the same sensitivity (because hexagonal holes can usually be made smaller than matched square holes, as the former do not share the latter's constraint of matching to the size of the detector pixels).

To first order the spatial resolution of either a hexagonal or square hole collimator is:

$$spatial\ resolution = 2 \cdot \frac{w}{h} \cdot \left(d + \frac{h}{2} \right) \qquad (1)$$

where w is the hole size, h the collimator height, and d the imaging distance. This equation thus loosely defines two imaging ranges: the near field, where the collimator geometry term ($h/2$) is dominant, and the far field, where the imaging distance d is dominant. An imaging distance equal to roughly half the collimator height—or about 10–15 mm for many of the compact collimators discussed in this paper—is the approximate crossover point between the two.

In the far field, the resolution is limited by the collimator aspect ratio (assuming the intrinsic resolution is sufficiently fine). In the near field, gamma rays from a point source centered over a collimator hole tend to penetrate exactly one hole, so if the collimator is matched to the detector pixel, the spatial resolution is determined by the pixel size and not the collimator aspect ratio. As the collimator sensitivity is approximately proportional to the square of the collimator aspect ratio for both the near and far field, the classical collimator resolution/sensitivity tradeoff does not hold in near field and finer resolution can be achieved without compromising sensitivity by reducing w and h proportionally. Given discrete square detector pixel elements (and assuming no collimator penetration), this advantage can be fully realized with a matched square hole collimator, but only partially realized with a hexagonal hole collimator (because geometric mismatch can allow two or more detector pixels to be exposed to gamma rays even if only one collimator hole is penetrated).

Potential for improving the resolution/sensitivity tradeoff thus exists when the object is in the near field of the collimator, which corresponds to an imaging distance of less than roughly half the height h of the collimator. Finer resolution in this region can be achieved by reducing the hole diameter w, but maintaining high sensitivity requires a corresponding reduction in h, which then reduces the extent of the near field. The collimator designs that we are currently exploring have a height h of 1.5–6.5 cm, limiting the imaging distance where these gains can be made to a maximum of 0.75–3.25 cm. As we wish to image breast lesions at distances as great as 5 cm, we cannot rely on the near field benefits to provide superior performance across the entire imaging range. Hence we must consider both near and far field performance when selecting a collimator geometry.

Measurements presented in this paper were made using hexagonal hole collimators primarily because of their present commercial availability. Our Monte Carlo simulations indicate that if the hexagonal collimator holes are small relative to pixel size (approximately: hole diameter < 0.5 * pixel size), the spatial resolution degradation due to the aliasing error between the collimator holes and detector pixels is small. This will be further addressed and quantified in subsections III.D and III.E.

III. DETECTOR IMAGING CHARACTERISTICS

A. Background Spectrum

We observe low count rates for the 3x4 array when there is no radiation source present. The average across all 12 pixels is 0.24 events/pixel/sec above a 50 keV threshold, and 0.015 counts/pixels/sec within the 126–154 keV energy window commonly used for ^{99m}Tc. This rate of background activity is consistent with cosmic ray flux. The summed spectrum for the entire array is shown in Figure 3.

B. Energy Resolution

The 12 pixels in the 3x4 detector array demonstrate an average room temperature energy resolution of 11.7±0.9% fwhm for the 140 keV emissions of ^{99m}Tc at amplifier shaping times of 8 μs (rise) and 24 μs (fall). However, the 53 nm thickness of the anti-reflective (AR) coating for this photodiode array was optimized for 410 nm light and not the 540 nm emissions of CsI(Tl), preventing complete collection of the scintillation photons. Calibration using the direct interaction of 5.9 keV ^{55}Fe gammas in silicon photodiodes (and assuming 3.6 eV per electron-hole pair generation) showed that the average signal amplitude in these measurements was 5400 e-. This value is very similar to the results reported in [16], wherein various cylindrical CsI(Tl) crystals (9 mm diameter, 1–9 mm height) read out with Hamamatsu photodiodes (S3590-3 and S2744-04) demonstrate an average signal level of 5387 e-.

We tested a second 3x4 detector array using an identical CsI(Tl) array coupled to a photodiode array with an AR coating optimized for CsI(Tl) (68 nm thickness, close to 1/4 the wavelength of 540 nm photons in a medium with an index of refraction of 1.9). The average signal amplitude increased to 6600 e-, and the average energy resolution dropped to 10.7±0.6% fwhm. A typical photopeak for this array is shown in Figure 4. The measurements of spatial resolution reported in the remainder of the paper, however, were made on the first detector array.

The choice of 8 μs shaping time (8 μs rise, 24 μs fall) provides the most accurate energy resolution despite the fact that the noise minimum for the amplifier/photodiode electronics occurs near 4 μs. The electronic noise at this shaping time is about 345 e- fwhm, compared to 390 e- fwhm at 8 μs. However, the slow decay components of CsI(Tl) scintillation light (as large as 3 μs decay rate) imply that more scintillation photons are collected at 8 μs than at 4 μs, and this increase in signal is larger than the associated
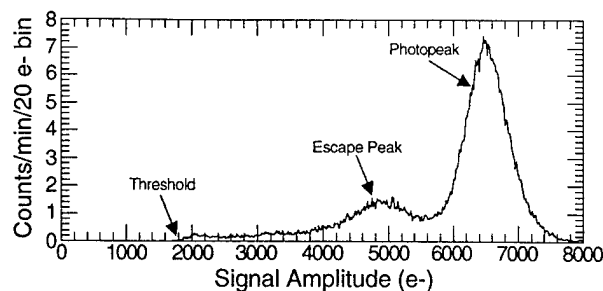
Figure 4. Room temperature ^{99m}Tc photopeak for a typical pixel. Amplifier shaping times were 8 μs rise and 24 μs fall. The signal amplitude is 6530 e- and the photopeak width is 680 e- fwhm, yielding an energy resolution of 10.4% fwhm. The average energy resolution for all array pixels is 10.7±0.6% fwhm.

increase in noise. At a shaping time of 8 μs, the electronic noise is 5.9% fwhm of the 6600 e- signal. The statistical noise is only 2.8% fwhm, leaving an additional 8.5% fwhm contribution (assumed to be due to the inhomogeneity of light collection in the CsI(Tl) crystals) in order to account for the average photopeak width of 10.7% fwhm.

There is potential to further improve the energy resolution and match or surpass the 8–9% fwhm achieved in traditional scintillation cameras. Signal amplitude can be increased by using higher quality CsI(Tl) arrays, as the crystals we used suffer from depth of interaction effects (*i.e.*, scintillation photons attenuate as they traverse the crystal) and suboptimal surface quality (preventing some scintillation photons from reaching the photodiode). Additionally, advances in the charge amplifier IC should reduce the electronic noise, and there remains the possibility of cooling the instrumentation to 5° C to lower dark currents and reduce the associated shot noise. Similar CsI(Tl)/photodiode technology in a cooled environment has demonstrated an energy resolution of 7.5% fwhm for the 122 keV emissions of ^{57}Co [11].

C. Intrinsic Spatial Resolution

When scanning a 2.5 mm diameter collimated ^{57}Co beam across the central row of four crystals in the CsI(Tl) array, we observe an average spatial resolution of 3.3 mm fwhm. Given the significant source diameter, this resolution is consistent with the crystal size of 3 mm and implies that electronic and Compton crosstalk are minimal. The responses of the four individual pixels are displayed in Figure 5.
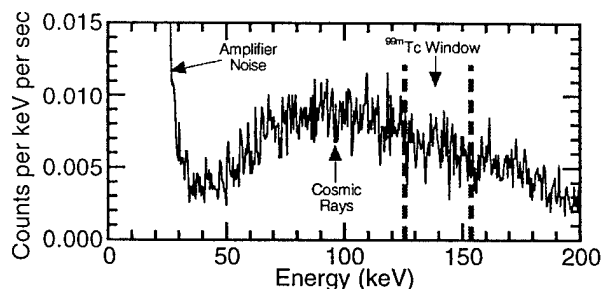

Figure 3. Background spectrum for all 12 pixels in the detector array. There are 0.24 counts/channel/sec above 50 keV, and 0.015 counts/channel/sec in the 136–154 keV ^{99m}Tc window.
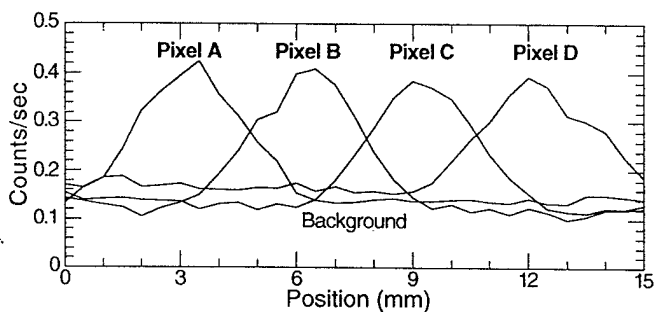
Figure 5. Response of the central row of four pixels to a 2.5 mm diameter ^{57}Co collimated beam scanned across the face of the CsI(Tl) array. The average spatial resolution is 3.3 mm fwhm. Significant background activity is apparent because the source activity was less than 20 nCi.

D. Spatial Resolution: High Resolution Collimator

The spatial resolution of the complete prototype module—including a high resolution collimator—was evaluated in air by scanning a 2 mm diameter uncollimated ^{99m}Tc source across the middle row of four pixels at imaging distances of 0.0, 2.5, and 5.0 cm (from the front face of the collimator). This is the imaging range of interest for clinical applications because with mild breast compression, most tumors to be imaged will be within 5 cm of the collimator surface. The collimator used has 1.5 mm diameter hexagonal holes and a length of 32 mm, yielding a sensitivity of about 4300 events/mCi/sec. The average spatial resolution of the four pixels is 4.1 mm fwhm at a distance of 0.0 cm, 4.8 mm fwhm at 2.5 cm, and 5.9 mm fwhm at 5.0 cm. Individual pixel responses are displayed in Figure 6.

Monte Carlo simulations of spatial resolution were performed to compare measured results with theoretical predictions, as well as to compare a standard hexagonal hole collimator to a collimator with square holes matched either 1-to-1 or 4-to-1 to the square CsI(Tl) crystals. The simulation determines the average spatial resolution across 25 different point source locations in order to prevent advantageous or disadvantageous positions from distorting the results. An infinitesimally small point source was assumed, septal penetration was not accounted for, and spatial resolutions in the x and y directions were weighted equally. The measured averages and simulated results are presented in Figure 7.

There is some discrepancy between the measured and simulated results for the hexagonal hole collimator. This can be partially accounted for by the fact that the experimental point source was 2 mm in diameter compared to an infinitesimally small simulated one, and by the existence of a ~1 cm air gap between the scintillator array and the collimator in the experimental setup but not in simulation (this gap was present due to bulky EM shielding that will be miniaturized in future modules). However, simulation of these effects indicates that they account for only 0.3 mm of the 0.9 mm spatial resolution difference between experiment and simulation at a 5 cm imaging distance. The remaining difference is likely the result of septal penetration and the penetration of gammas through part of one crystal before being absorbed in another crystal, neither of which were included in simulation.
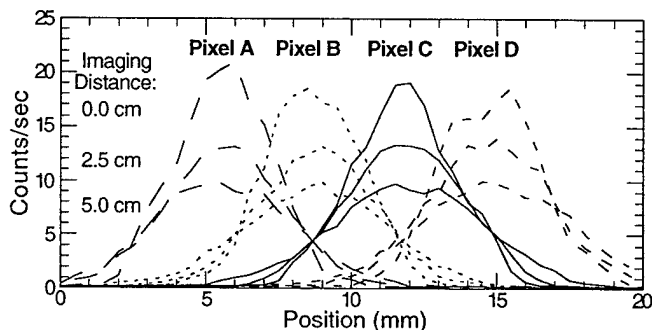

Figure 6. Response of the central row of four pixels behind a high resolution hexagonal hole collimator to a 2.0 mm diameter uncollimated ^{99m}Tc source scanned across at imaging distances of 0.0, 2.5, and 5.0 cm. The average spatial resolution at these distances is 4.1 mm fwhm, 4.8 mm fwhm, and 5.9 mm fwhm, respectively. Measurements were performed in air. The collimator has a sensitivity of 4300 events/mCi/sec.
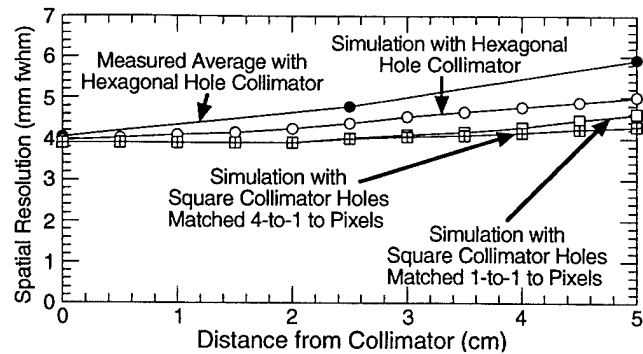

Figure 7. Average spatial resolution versus imaging distance for measured (see Figure 6) and simulated results with high resolution collimators. The simulated hexagonal hole collimator has an identical geometry to the experimental collimator, the 1-to-1 matched square hole collimator is 66 mm long with 2.8x2.8 mm^2 holes (0.2 mm septal thickness makes unit cells 3.0x3.0 mm^2), and the 4-to-1 matched square hole collimator is 30 mm long with 1.3x1.3 mm^2 holes (0.2 mm septal thickness makes unit cells 1.5x1.5 mm^2). All collimators have sensitivities of about 4300 events/mCi/sec.

The simulation results of Figure 7 suggest that a 1-to-1 matched square hole collimator provides slightly better spatial resolution than a hexagonal one. The average improvement across the 0–5 cm imaging range is 0.32 mm fwhm. This comes at the expense of a collimator that needs to be quite long (66 mm) in order to achieve comparable sensitivity, which is contrary to the goal of compact design. Simulations suggest that using a comparable sensitivity 4-to-1 matched square hole collimator improves the average spatial resolution by an additional 0.08 mm fwhm and requires a collimator length of only 30 mm. A hexagonal hole collimator with the same sensitivity but a more preferable geometry than the one we used (1.0 mm holes instead of 1.5 mm holes) would still be shorter at 20 mm.

In simulations the hexagonal hole collimator exhibits more dependence on source location than do either of the square hole collimators. The spatial resolution of the hexagonal hole collimator over the 25 source locations demonstrates a standard deviation of 0.47 mm (this is the average of the individual standard deviations at different imaging distances in the 0–5 cm range). The standard deviation for both the 1-to-1 and 4-to-1 square hole collimators is 0.45 mm. Despite this very minor difference, there are extreme cases when the spatial resolution of the hexagonal hole collimator is as high as 7.0 mm fwhm (2.1 mm above the average), while for the square hole collimators the worst resolution was 4.9 mm fwhm (0.5 mm above the average).

Our simulations suggest that the aliasing artifacts that result from shape mismatch between hexagonal collimator holes and square scintillation crystals decrease with decreasing hexagonal hole diameter, and the majority of these aliasing artifacts become very small once the diameter is less than half the pixel size. Lower limits on the hole diameter are set, however, by manufacturing limitations and by the fact that septal thickness cannot be scaled down along with hole diameter. Collimators with hexagonal holes as small as 1.0 mm are readily available from industry and demonstrate promising spatial resolution and sensitivity characteristics with a discrete detector array when simulated.

E. Spatial Resolution: High Sensitivity Collimator

An extremely important consideration in collimator design is the classic tradeoff between spatial resolution and sensitivity. When imaging in the far field, the sensitivity is roughly proportional to the spatial resolution squared, hence a small degradation in the collimator resolution can yield a significant sensitivity improvement. We repeated the measurements described in subsection III.D using a hexagonal hole collimator with nearly twice the sensitivity of the high resolution collimator. This high sensitivity collimator has 2.0 mm diameter holes, a length of 32 mm, and a sensitivity of 8200 events/mCi/sec. The average observed spatial resolution is 4.3 mm fwhm at a 0.0 cm imaging distance, 5.5 mm fwhm at 2.5 cm, and 6.5 mm fwhm at 5.0 cm. Observed and simulated spatial resolutions for this collimator, as well as simulations for 1-to-1 and 4-to-1 matched square hole collimators of comparable sensitivity, are shown in Figure 8.

When using the high sensitivity hexagonal hole collimator, the measured spatial resolution degrades an average of 0.50 mm fwhm compared to the high resolution collimator. The associated doubling in sensitivity, however, would decrease patient dose, decrease imaging time, and/or improve counting statistics. The high sensitivity hexagonal hole collimator demonstrates a worse spatial resolution in measurements than in simulation for the same reasons discussed in subsection III.D.

The simulated 1-to-1 matched square hole collimator (47 mm long) demonstrates an average spatial resolution improvement of 0.31 mm fwhm compared to the simulated hexagonal hole collimator, while the 4-to-1 square hole collimator (21 mm long) exhibits a further improvement of 0.17 mm fwhm. As with the high resolution collimators, a high sensitivity hexagonal hole collimator with 1.0 mm holes would be shorter yet at 15 mm.

The standard deviation of the spatial resolution demonstrated by the simulated hexagonal hole collimator averages 0.49 mm, compared to 0.37 mm and 0.38 mm for the 1-to-1 and 4-to-1 square hole collimators, respectively. A
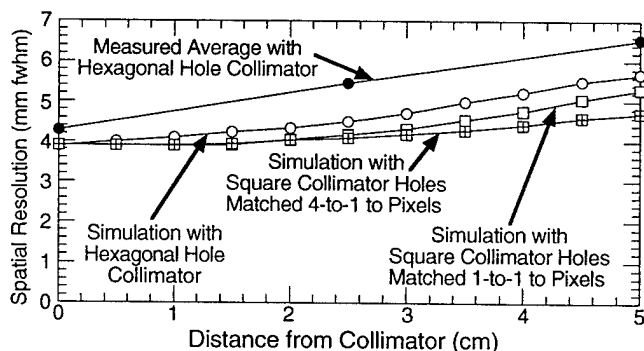

Figure 8. Average spatial resolution versus imaging distance for high sensitivity collimators. The simulated hexagonal hole collimator has an identical geometry to the experimental collimator, the 1-to-1 matched square hole collimator is 48 mm long with 2.8x2.8 mm^2 holes (0.2 mm septal thickness makes unit cells 3.0x3.0 mm^2), and the 4-to-1 matched square hole collimator is 21 mm long with 1.3x1.3 mm^2 holes (0.2 mm septal thickness makes unit cells 1.5x1.5 mm^2). All collimators have sensitivities of about 8200 events/mCi/sec.

few extreme cases are evident, as the maximum spatial resolution of the hexagonal hole collimator is 8.5 mm fwhm (2.8 mm above average), whereas the worst resolution exhibited by either square hole collimator is 5.9 mm fwhm (0.6 mm above average).

IV. CONCLUSIONS

The two advances that now make discrete scintillation camera technology a viable option for scintimammography applications are the low leakage current (~50 pA/pixel) photodiode arrays and the custom IC readout of the photodiode signals. Low leakage current is critical to achieving low electronic noise (especially at longer shaping times), which in turn improves the signal-to-noise ratio and hence the energy resolution. Custom IC readout of the photodiode arrays is important to achieving a compact, cost effective design, because with the many pixels that will be present in a complete camera, discrete electronics become prohibitively bulky and expensive.

The prototype 3x4 pixel discrete scintillation camera module demonstrates good energy and spatial resolution characteristics that suggest a full camera consisting of an array of modules would prove a successful scintimammography imaging device. An average energy resolution of 10.7% fwhm was demonstrated for ^{99m}Tc, and observations by other researchers indicate that better CsI(Tl) crystals and cooled electronics can yield an energy resolution as low as 7.5% fwhm. There is some hope that this discrete scintillation camera technology can meet or even surpass the 8–9% fwhm energy resolution typically demonstrated by conventional scintillation cameras.

The spatial resolution observed when using a high resolution hexagonal hole collimator (4300 events/mCi/sec) is 5.9 mm fwhm at 5 cm (the anticipated maximum tumor-to-camera imaging distance), and simulations suggest the potential to improve to less than 5 mm fwhm. This good spatial resolution is notable because scintimammography with conventional scintillation cameras is poor at detecting tumors less than 1 cm in diameter. The proposed discrete, compact camera should be able to see significantly smaller lesions.

Collimator design has a crucial impact on camera performance. With hexagonal hole collimators, increasing the sensitivity from 4300 to 8200 events/mCi/sec degrades the spatial resolution by only about 0.5 mm fwhm over the 0–5 cm imaging range, from 4.1–5.9 mm fwhm to 4.3–6.5 mm fwhm. Simulations suggest that the choice of a 1-to-1 matched square hole collimator over a hexagonal one of comparable sensitivity improves spatial resolution by an average of about 0.4 mm fwhm, but at the cost of a longer, less compact collimator. A 4-to-1 matched square hole collimator further improves spatial resolution by about 0.1 mm and allows a reasonably short collimator. The spatial resolution of both square hole collimator configurations demonstrate less dependence on source location than does that of a comparable hexagonal hole collimator. The hexagonal collimator should have a more uniform septal penetration pattern, but this effect was not included in the simulations.

The advantages and disadvantages inherent in the choice between hexagonal and matched square hole collimators,

however, will have a much smaller impact on the ability of a camera to detect breast lesions than will the traditional tradeoff between spatial resolution and sensitivity. This optimization is heavily dependent on assumptions regarding lesion sizes, relative tracer uptake ratios, imaging distances, and imaging time, making it beyond the scope of this paper.

V. ACKNOWLEDGMENTS

VI. REFERENCES

[1] R. Taillefer, A. Robidoux, S. Turpin, et al., "Detection of axillary lymph node involvement with Tc-99m-sestamibi imaging in patients with primary breast cancer," *J Nucl Med*, vol. 37, pp. P75, 1996.

[2] I. Khalkhali, J. Villanueva-Meyer, S.L. Edell, et al., "Diagnostic accuracy of Tc-99m Sestamibi breast imaging in breast cancer detection," *J Nucl Med*, vol. 37, pp. 74P, 1996.

[3] S. Piccolo, S. Lastoria, C. Mainolfi, et al., "Technetium-99m-methylene diphosphonate scintimammography to image primary breast cancer," *J Nucl Med*, vol. 36, pp. 718–724, 1995.

[4] H. Palmedo, H.H. Biersack, S. Lastoria, et al., "Scintimammography with Tc-99m MIBI for breast cancer detection: results of the prospective European multicenter trial," *J Nucl Med*, vol. 38, pp. 20–21P, 1996.

[5] I Khalkhali, J. Villanueva-Meyer, S.L. Edell, et al., "Impact of breast density on the diagnostic accuracy of Tc-99m sestamibi breast imaging in the detection of breast cancer," *J Nucl Med*, vol. 37, pp. 74–75P, 1996.

[6] C.H. Kao, S.J. Wang, and S.H. Yeh, "Tc-99m MIBI uptake in breast carcinoma and axillary lymph node metastases," *Clin Nucl Med*, vol. 19, pp. 898–900, 1994.

[7] H. Palmedo, A. Schomburg, F. Grunwald, et al., "Technetium-99m-scintimammography for suspicious breast lesions," *J Nucl Med*, vol. 37, pp. 626–630, 1996.

[8] W.W.M. Lam, W.T. Yang, Y.L. Chan, et al., "Detection of axillary lymph node metastases in breast carcinoma by technetium-99m sestamibi breast scintigraphy, ultrasound, and conventional mammography," Eur J Nucl Med, vol. 23, pp. 498–503, 1996.

[9] J. Strobel, N.H. Clinthorne, and W.L. Rogers, "Design studies for a cesium iodide silicon photodiode gamma camera," *J Nucl Med*, vol. 38, pp. 31P, 1997.

[10] C.S. Levin, E.J. Hoffman, M.P. Tornai, et al., "Design of a small scintillation camera with photodiode readout for imaging malignant breast tumors," *J Nucl Med*, vol. 37, pp. 52P, 1996.

[11] B.E. Patt, J.S. Iwanczyk, M.P. Tornai, et al., "Dedicated breast imaging system based on a novel solid state detector array," *J Nucl Med*, vol. 38, pp. 142P, 1997.

[12] S.E. Holland, N.W. Wang, and W.W. Moses, "Development of low noise, back-side illuminated silicon photodiode arrays," *IEEE Trans Nucl Sci*, NS-44, pp. 443–447, 1997.

[13] W.W. Moses, I. Kipnis, and M.H. Ho, "A 16-channel charge sensitive amplifier IC for a PIN photodiode array based PET detector module," *IEEE Trans Nucl Sci*, NS-41, pp. 1469–1472, 1994.

[14] W.W. Moses, I. Kipnis, and M.H. Ho, "A 'winner-take-all' IC for determining the crystal of interaction in PET detectors," *IEEE Trans Nucl Sci*, NS-43, pp. 1615–1618, 1996.

[15] M.P. Tornai, B.E. Patt, J.S. Iwanczyk, C.S. Levin, et al., "Discrete scintillator coupled mercuric iodide photodetector arrays for breast imaging," *IEEE Trans Nucl Sci*, NS-44, pp. 1127–33, 1997.

[16] M. Moszynski, M. Kapusta, M. Mayhugh, et al., "Absolute Light Output of Scintillators," *IEEE Trans Nucl Sci*, NS-44, pp. 1051–1061, 1997.